Semiannual Report

Under
Contract # NAG - 5 - 1010
National Aeronautics and Space Administration

Improvement and extension of a radar forest backscattering model

Prepared by:
David S. Simonett
Yong Wang

DEPARTMENT OF GEOGRAPHY
UNIVERSITY OF CALIFORNIA SANTA BARBARA

May 10, 1989

1. Introduction

Radar modeling of mangal forest stands, in the Sundarbans area of Southern Bangladesh, has been developed. The modeling employs radar system parameters with forest data on tree height, spacing, biomass, species combinations, and water (including slightly conductive water) content both in leaves and trunks of the mangal. For Sundri and Gewa tropical mangal forests, six model components are proposed, which are required to explain the contributions of various forest species combinations in the attenuation and scattering of mangal vegetated nonflooded or flooded surfaces. Statistical data of simulated images have been compared with those of SIR-B images both to refine the modeling procedures and to appropriately characterize the model output. The possibility of delineation of flooded or nonflooded boundaries is discussed.

2. Characteristics of the Study Area

2.1. Characteristics of Mangal Forests in Southern Bangladesh

2.1.1. Individual Organs of a Gewa and a Sundri Tree

Gewa *(Excoecaria agallocha)* and Sundri *(Heritiera minor Syn. H. formes)* are mangrove species. The shoots are mostly orthotropic with infrequent diffuse branches, which sometimes may branch from the base and shrub-like form. Leaves are simple in shapes; and broad in size (Tomlinson, 1986). Gewa lacks any elaborated aerial part or pneumatophores, which function to supply oxygen to the roots at high tide. Sundri does have pneumatophores.

Gewa yields a light, yellowish-white, fine-textured, and not very durable wood, mainly used for general carpentry work and toys, and (especially) for newsprint and matches (FAO, 1981).

Sundri yields a heavy, dark red, fine-textured, strong and extremely durable wood, which is used for boat building, heavy construction work, beams, and house-posts (FAO, 1981).

2.1.2. Whole Gewa and Sundri Trees

A mature Gewa tree, as shown in Figure 2.1, grows intermittently and irregularly, up to 20 meters high for a mature tree. Branching is diffuse, irregular, and by prolepsis. Canopy is dense. Models of geometric shapes and structure for different ages of Gewa trees were described by Tomlinson (1986): with continuous growth of the trunk repeated in the branches, which have lateral inflorescences.

A mature Sundri tree, as shown in Figure 2.2, is about 10 to 25 meters tall, and low-branched. The branches are thick and crooked. Canopy is very dense. Tomlinson (1986) also introduced a series of geometric models for Sundri trees of different ages: with rhythmic growth, undifferentiated branches, and lateral inflorescences.

2.1.3. Gewa and Sundri Forest Stands

Gewa and Sundri forests occur essentially and dominantly at the tidal mouth of the Baleswar River in southern Bangladesh, which belong to closed broadleaved woody tropical rain forests (FAO,

1981). Most of the mouth areas are frequently flooded by fresh water during the monsoon rains (May - June to October - November, Chapman, 1977), with salt water intrusion during the rest of a year. Gewa and Sundri forests are very difficult of access with soft footing, and have extremely high canopy and stem densities. Estimations of the mangrove forests in this area are about 590,000 hectares (FAO, 1982), which contribute very important forest resources and environmental protection for Bangladesh: they provide marketable products, and also play roles as buffers for storm surges, and tidal waves coming from the Bay of Bengal (Imhoff et al., 1986). The forest becomes poorer and more open as one processes towards the sea or salt water intrusion area. Sundri mainly lives in the area where the fresh water is available, and becomes smaller and less abundant as one goes from fresh water areas towards salt water areas. Gewa is mainly in the saltwater area, and also there are some Gewa forests in the fresh area (FAO, 1982).

2.2. Ground Surfaces

The Delta soil is a clay loam lying over alternating layers of clay and sand, highly saturated with exchangeable bases (Na^+, Ca^{++}, K^+, etc.). The salinity of the soil varies seasonally as a result of the changing balance of fresh water and salt water. Chapman (1977) pointed out that there is a very high salinity at the beginning of the dry season, and this factor considerably limits the development, maintenance, or regeneration of the less halophilous species such as Sundri, which is on the way to extinction because of excessive salt water intrusion. During the rainy season (when the SIR-B images were obtained), the salinity will be low.

3. Analysis of Ground Truth Data

Ground truth data of Sundri and Gewa mangal forest in our southern Bangladesh research site were originally collected by a NASA and Bangladesh science team concurrently with the SIR-B Mission in October, 1984; and subsequently by Chaffey, et al., (1985). All these data were prepared by averaging measurements made for inventory plots each 100 * 100 meters (one hectare) in size, consisting of:

a. a digitized forest stand map;

b. DBH count distributions by DBH segments;

c. tree heights and canopy depths by their DBHs;

d. canopy biomass of in each DBH segment; and

e. gravimetric moisture content of canopies and trunks.

3.1. The Digitized Forest Stand Map

The digitized forest stand map containing different Sundri and Gewa stands in the test site was geo-registered with the SIR-B images obtained in October, 1984. The number of pixels and names of each forest stand are shown in Table 3.1. These stands have different tree densities per unit area for each DBH segment. The digitized forest stand map is used as a mask to locate and to extract each forest stand data from the SIR-B images. The ground surface is either flooded or nonflooded.

3.2. DBH Count Distributions by DBH Segments per Hectare

DBH count distributions by DBH segments per hectare are shown in Table 3.2, which are used to generate random tree trunk distributions with varying DBHs in one simulated stand area such as twenty hectares (assumed in our modeling). Based on both the combination of two Sundri and Gewa species and the random distributions of the tree trunks, tree counts for each DBH segment of Sundri and Gewa in each pixel in the stand area are created.

3.3. Tree Heights and Canopy Depths by Their DBHs

Tree heights and canopy depths determined from their DBHs are obtained by regression, from the data collected by a NASA and Bangladesh science team in October 1984, employing the data of tree heights, canopy depths and DBHs; and these regression models are shown in Table 3.3. These regression models were employed to calculate each tree height and mean canopy depth in each simulated pixel in a forest stands, using the DBH counts for each DBH segment in each simulated image pixel. The effective trunk heights, or dielectric cylinder lengths, used in the modeling were defined as the total tree height minus two thirds of the corresponding mean canopy depth.

3.4. Mean Canopy Biomass in Each DBH Segment

Mean canopy biomass value in each DBH segment is calculated by dividing the total biomass (kg) by the tree numbers in each DBH segment, as shown in Table 3.4. The mean canopy biomass data in each simulated pixel is computed by the total trees (with different DBHs) in this pixel multiplying by the mean canopy biomass value for corresponding DBH segments. The total biomass is then converted to volume ratio (m^3/m^3) by 1) the total biomass (Sundri and Gewa respectively) dividing by their specific weight (kg/m^3), which gives the total canopy volume of the Sundri and the Gewa canopy; 2) the total canopy volumes (Sundri and Gewa canopy volumes) are divided by the total volume which is defined as pixel size times the mean canopy depth in this pixel. Thus the converted ratio is a volume occupied by the tree canopies to the total volume. This volume ratio parameter has been employed as an input parameter to compute the attenuation coefficient, and the scattering coefficient of Sundri and Gewa trees for each pixel using models developed by Ulaby, et al., (1986). The biomass varies as a result of variation in both the total tree numbers in each pixel and the tree number in each DBH segment.

3.5. Gravimetric Moisture Contents of Canopies and Trunks

Gravimetric moisture contents of canopies and trunks are derived from dry and wet biomass data. Because of a lack of explicit data to separate Gewa and Sundri, we assume the water content in the canopies and trunks to be the same for each species. The water contents are: canopy, $\mu = 0.402668$, $\sigma = 0.038955$; and trunk, $\mu = 0.453775$, $\sigma = 0.057921$. These data are used to compute the dielectric constants of the canopies and the trunks following Ulaby and El-Rayes (1987).

4. Radar Models of Sundri and Gewa Forest Stands

Based on the above analysis, six model components are proposed, as shown in Figure 4.1 (see also Wang, et al., 1989):

1 Direct backscattering from ground surface (short form σ^o_{dbs}),

2 Direct volume scattering from upper canopy* (short form σ^o_{vsu}),

3 Direct volume scattering from lower canopy* (σ^o_{vsl}),

4 Interaction of trunk/ground forward reflection (σ^o_{itg}),

5 Interaction of ground/upper canopy forward scattering (σ^o_{guc}), and

6 Interaction of ground/lower canopy forward scattering (σ^o_{glc}).

The total radar return is

$$\sigma^o_{tot} = \sigma^o_{dbs} + \sigma^o_{vsu} + \sigma^o_{vsl} + \sigma^o_{itg} + \sigma^o_{guc} + \sigma^o_{glc}$$

σ^o_{dbs}: the small perturbation model, used for both flooded and nonflooded surfaces, is (Dobson and Ulaby, 1986):

$$\sigma^o_{dbs} = \frac{A_s}{A} \times 4(k_o h)^2 (k_o l)^2 \cos^4\theta_i \, exp\,[-(k_o l \sin\theta_i)^2] \, |R_{hh}(\theta_i)|^2$$

where the θ_i is the radar incidence angle, and k_o the radar wavenumber ($\frac{2\pi}{\lambda}$; λ is the radar wavelength). A_s is the surface area not shadowed by trunks and A is the pixel area. h and l are the rms roughness and surface correlation length, which are assumed (no measurement data available) as: flooded surface, h_{sea} = 0.01m, l_{sea} = 0.15m; nonflooded surface, h_{sur} = 0.02m, and l_{sur} = 0.075m, respectively. The basis for these assumptions lies in the requirements of the small perturbation model, and the either flooded or nonflooded surface condition. $R_{hh}(\theta_i)$, the Fresnel reflectance coefficient of the surface for HH polarization, is (μ_r=1.0 is assumed):

$$R_{hh}(\theta_i) = \frac{\cos\theta_i - \sqrt{\varepsilon_r - \sin^2\theta_i}}{\cos\theta_i + \sqrt{\varepsilon_r - \sin^2\theta_i}}$$

where the $\varepsilon_r = \varepsilon' - j\,\varepsilon''$ is the relative dielectric constants of the surfaces (flooded and nonflooded). The dielectric constant of the flooded surface is assumed to be equivalent to 1 % salinity, because of extensive dilution during the monsoonal rainy season (when the SIR-B images were obtained). The dielectric constant of the ground surface is derived from the mixed model of Ulaby, et al., (1986).

σ^o_{vsu}: the water cloud model (Attema and Ulaby, 1978) is chosen: this model is simple and functional; no measurement data on orientations of branches or leaves are available; and only HH polarization is studied. The model is:

$$\sigma^o_{vsu} = \frac{\eta_u \cos\theta_i}{2\kappa_u} [1 - exp\,(-2\kappa_u h_{cu} \sec\theta_i)]$$

*: Upper and lower canopies are defined as the canopies of trees whose DBH's are respectively >= 5.0 cm or < 5.0 cm; the latter is also termed regrowth.

in which h_{cu} is the mean upper canopy depth in each simulated pixel. κ_u is the upper canopy extinction coefficient, which is derived by a volume ratio and the canopy dielectric constants (Ulaby, et al., 1986). η_u is a volume scattering coefficient of the upper canopy layer. The ratio of the volume scattering coefficient to the extinction coefficient is assumed as 0.3, and 0.4 for the upper and the lower canopy layers respectively, because the lower canopy is denser than the upper canopy. These values are higher than those used by Sun and Simonett (1988): the mangal forest canopy is much denser than the pine forests of northern California which they studied; and Gewa especially may also have a slight salinity inside leaves and branches (Snedaker, personal communication, April, 1989). In addition, the sensitivity of the model to change in the ratio is low as shown by Richards, et al. (1987). Using the ratio and the attenuation coefficient computed in each pixel, η_u and η_l are then solved.

σ^o_{vsl}: basically is the same model as σ^o_{vsu}, but with different mean canopy depths; and canopy densities or volume ratios, which produces different attenuation coefficients and scattering coefficients.

σ^o_{itg}: is the specular scattering coefficient of dielectric cylinders with finite lengths (Ruck, et al., 1970) multiplied by the reflection coefficient of the surfaces (flooded or nonflooded). Tree trunks are modeled as dielectric cylinders with smooth surfaces. If a dielectric cylinder length is much greater than the wavelength ($l \gg 2\lambda$), the scattered field from the cylinder propagates in $\theta_s = 90.0_o - \theta_i$, and azimuth angle from 0^o to 360^o, where the θ_s is a scattering angle. The bistatic scattering cross section of the cylinder with finite length (Ruck, et al., p. 304, 1970) is:

$$\sigma_{hh}\ (\theta_i, \theta_s, \phi_s) = \frac{k_0 l^2}{\pi}\cos^2\theta_s \sigma^c_{hh}(\theta_i, \phi_s) \left[\frac{\sin(k_0(\cos\theta_i + \sin\theta_s)l/2)}{k_0(\cos\theta_i + \sin\theta_s)l/2}\right]^2$$

where l is the cylinder length, and is calculated from the regression models on tree heights. The effective trunk length or the dielectric cylinder length is the total tree length minus two thirds of its canopy depth. $\sigma^c\ (\theta_i, \phi_s)$ is the scatter width for an infinitely long cylinder at oblique incidence, which is (for HH polarization) (Ruck, et al., p.271, 1970):

$$\sigma^c_{hh}(\theta_i, \phi_s) = \frac{4}{k_0 \sin^2\theta_i}\left|\sum_{n=-\infty}^{\infty}(-1)^n C_n e^{in\phi_s}\right|^2$$

where the constant C_n is a function of the cylinder radius, the material, as well as the shapes or boundaries. The ϕ_s is the scattering azimuth angle. When $\phi_s = 0.0^o$ and $\theta_s = -(90.0^o - \theta_i)$, this is the specular scattering. When $\phi_s = 180.0^o$ and $\theta_s = -(90.0^o - \theta_i)$, this is the forward scattering. For the specular case, the scattering coefficient is:

$$\sigma_{hh}\ (\theta_i, 90.0^o - \theta_i, 0.0) = \frac{k_0 l^2}{\pi}\sin^2\theta_i \sigma^c_{hh}(\theta_i, 0.0)$$

For the flooded and nonflooded surfaces, the Fresnel reflection coefficients are modified for slightly rough surfaces (Ruck, et al., 1970) as:

$$R^r_{hh}(\theta_i) = R_{hh}(\theta_i)\exp[-2(k_o h\cos\theta_i)^2]$$

The dielectric constants of the Gewa and Sundri trunks are about (22.0 - j 7.0); (18.5 - j 5.0), which are derived from the model developed by Ulaby and El-Rayes (1987) with gravimetric moisture

content, equivalent salinity, and temperature as input. These values are slightly higher than those measured by Ulaby and Jedlicka (1984); and El-Rayes and Ulaby (1987), because the mangal has a higher salinity inside its leaves and trunks.

For one single tree (or the k^{th} tree), the interaction of the ground surface/trunk is:

$$\sigma^o_{itg_k} = 2.0 \times R^r_{hh}(\theta_i) \times \sigma_{hh}\ (\theta_i,\ 90.0^o - \theta_i,\ 0.0)$$

where we use 2.0 to account for the double paths from ground surface/trunk, and trunk/ground surface. Also, the phase produced by range difference is taken into account, or each σ^o_{itg} is summed by given a random phase for each tree trunk in every single simulated pixel because of the assumption of random location of each tree in every single simulated pixel, which is:

$$\sigma^o_{itg} = \left| \sum_{k=1}^{n} \sqrt{\sigma^o_{itg_k}} \times e^{j\phi_k} \right|^2$$

where the n is the total number of trees in one simulated pixel, and the ϕ_k is the random phase of the k^{th} trunk/ground surface interaction term.

σ^o_{guc}: the same model as used by Sun and Simonett (1988), originally derived from Engheta and Elachi (1982):

$$\sigma^o_{guc} = h_{cu}\eta_u\, |R^r_{hh}(\theta_i)|^2 [2 + |R^r_{hh}(\theta_i)|^2 \exp(-\alpha_u) sinh(\alpha_u)/\alpha_u]$$

where $\alpha_u = \kappa_u h_{cu} \sec\theta_i$.

σ^o_{glc}: a similar model as above, except for different densities, mean canopy depth, and equivalent dielectric constants.

It should be noted that all these model components may or may not be attenuated by the upper and/or the lower canopies, depending on their presence or not. The attenuation coefficients for the presence of an upper canopy layer are:

$$TAU_u = \exp(-2.0\kappa_u h_{cu} \sec\theta_i)$$

and for the lower canopy layer:

$$TAU_l = \exp(-2.0\kappa_l h_{cl} \sec\theta_i)$$

where the κ_u and κ_l are the extinction coefficients of the upper and the lower canopy layers, respectively. h_{cu} and h_{cl} are the mean canopy depths in each simulated pixel for the upper and lower canopies.

5. Discussion

The subareas of three forest stands (Table 3.1) are extracted from SIR-B images (DT 120 incidence angle 26°; and DT 104 incidence angle 46°; see also Imhoff, et al., 1986), and the DNs of the images converted to relative radar backscattering coefficients (dB) by

$$\sigma^o = 10 * log(DN^2 - C_{1i}) - C_{2i}$$

where i = 1, 2, corresponding to DT 120 and DT 104. C_{1i} are the noise levels, C_{2i} constants for calibration. Both C_{1i} and C_{2i} were provided by Marc Imhoff (1988, personal communication), as shown in Table 5.1.

The boxplots of SIR-B images are shown in Figures 5.1 (DT 120) and 5.2 (DT 104), with the modeling results plotted to the right. From these Figures, we conclude that:

5.1. The Fit of the Models to the SIR-B Images

The distributions of radar returns for each stand and two incidence angles are almost identical. The fit of the model to the image data is good. There are differences in the absolute values (the returns from our model are about 5 to 8 dB higher than the returns of SIR-B images). The reason may be that the models are theoretical solutions and each model component is incoherently added, which could produce higher values. Also, the C_{2i} (i = 1, 2, provided by Marc Imhoff, 1988, personal communication) may by a littler bit too large.

5.2. Radar Returns of Nonflooded and Flooded Areas

At 26° and 46° degree incidence angles, the returns for both SIR-B images and modeling results from flooded surfaces are slightly higher than those from nonflooded surfaces. However, the difference appears to be slight because of strong attenuation by the dense canopies. The return difference from large to small of each stand is in the order of GS (highest), G, and SG (lowest) stands. There is insufficient data in Table 3.2 to account for these differences.

5.3. Differences in Radar Returns Between Different Stands

There are no obvious differences between different stands. We reason as follows: a) each stand is a mix of Sundri and Gewa in varying proportions; b) the number of stems is very large, which is of importance in both enhancing the σ^o_{itg} (because of the large number of trunks), and in attenuation (because of the very dense canopy); and c) the structure of Sundri and Gewa are similar to each other (Tomlinson, 1986). The returns from SG stands may be the lowest because the density of the canopy layer may be marginally greater than that of other canopies (see Table 3.2).

5.4. Radar Returns between Two Different Incidence Angles

The mean (or median) are almost the same, but with greater variance at the smaller incidence angle for which there is a shorter path length through the canopy, yielding less attenuation for the σ^o_{itg} term. The σ^o_{itg} is the main component producing the variance for mangal: a similar conclusion was reached by Sun and Simonett (1988) for pine forest.

5.5. Penetration of the Canopy and Delineation of Flooded Areas

There is penetration to some degree, but it is not very obvious. The difference of radar returns between the flooded and nonflooded areas of both the SIR-B images and modeling results are around 0.5 - 2.0 dB. This is probably not large enough to delineate the flooded boundaries with confidence, because of the high intrinsic variance in SIR-B images.

5.6. Relative Importance of the Six Model Components

The dominant model components are σ^o_{itg}, σ^o_{vsu}, and σ^o_{vsl}, which are roughly equal for nonflooded surfaces. For flooded surfaces σ^o_{itg} is increased, and σ^o_{vsu} and σ^o_{vul} are unchanged. In areas where there are some natural clearings which lack the dense canopy layer, σ^o_{itg} is clearly dominant. We especially note the high returns from those forest edges which face the radar illumination direction. This feature has also been widely observed in short wavelength images of forest edges.

6. Bibliography

Attema, C. F. and F. T. Ulaby, (1978), "Vegetation modeled as a water cloud", *Radio Science*, vol. 13, pp. 357 - 364.

Chaffey, D. R., F. R. Miller, and J. H. Sandom, (1985), "A forest inventory of the Sundarbans, Bangladesh", *British Overseas Development Administration Project # 140, Land Resource Development Center*, Tolworth, Surbiton, Surrey, England.

Chapman, V. J. (1977), "*Wet coastal ecosystems, Ecosystems of the world 1*", Elsevier Scientific Publication Company.

Dobson, M. C. and F. T. Ulaby, (1986), "Preliminary evaluation of the SIR-B response to soil moisture, surface roughness, and crop canopy cover", *IEEE Transactions on Geoscience and Remote Sensing*, vol. GE-24, no. 4, pp. 517-526.

El-Rayes, M. A. and F. T. Ulaby, (1987), "Microwave dielectric spectrum of vegetation - Part I: experimental observations", *IEEE Transactions on Geoscience and Remote Sensing*, vol. GE-25, no. 5, pp. 541-549.

Engheta, N. and C. Elachi, (1982), "Radar scattering from a diffuse vegetation layer over a smooth surface", *IEEE Transactions on Geoscience and Remote Sensing*, vol. GE-20, no. 2, pp 212-216.

FAO, Food and Agriculture Organization of the United Nations, (1981), "*Tropical resources assessment project (in the framework of the global environment monitoring system - GEMS)*", *Forest resources of tropical Asia.*

FAO, Food and Agriculture Organization of the United Nations, (1982), "*Management and utilization of mangroves in Asia and the Pacific*".

Fosbery, F. R., (1971), "Mangroves v. tidal waves", *Biol. Conserv.*, 4: 38-39.

Imhoff, M. L., M. Story, C. Vermillion, F. Khan, and F. Polcyn, (1986), "Forest canopy characterization and vegetation penetration assessment with space-borne radar", *IEEE Transactions on Geoscience and Remote Sensing*, vol. GE-24, no. 4, pp. 535-542.

Richards, J. A., G. Q. Sun and D. S. Simonett, (1987), "L-band radar backscatter modeling of forest stands", *IEEE Transactions on Geoscience and Remote Sensing*, vol. GE-25, no. 4, pp. 487-498.

Ross, J., (1981), *The radiation regime and architecture of plant stands*, Dr W. Junk Publishers.

Ruck, G. T., D. E. Barrick, W. D. Stuart, and C. K. Krichbaum, (1970), "*Radar cross section handbook*", Plenum Press, New York.

Simonett, David. S., Alan H. Strahler, Guoqing Sun, and Yong Wang, (1987), "Radar Froest Modeling: Potentials, Problems, Applications, Models", *Advances in Digital Image Processing*, Proceedings of the Annual Conference of the Remote Sensing Society, Norttingham, England, Sept. 1987, pp. 256 - 269.

Sun, G. Q. and D. S. Simonett, (1988), "Simulation of L-band HH radar backscatter from coniferous forest stands: a comparison with SIR-B data", *International Journal of Remote Sensing*, vol. 9, no. 5, pp. 907 - 925.

Tomlinson, P. B., (1986), "*The botany of mangroves*", Cambridge University Press.

Ulaby, F. T., R. K. Moore, and A. K. Fung, (1986), "*Microwave Remote Sensing, vol. III: From theory to application*", Artech House.

Ulaby, F. T and R. P. Jedlicka, (1984), "Microwave dielectric properties of plant materials", *IEEE Transactions on Geoscience and Remote Sensing*, vol. GE-22, no. 4, pp. 406-414.

Ulaby, F. T and M. A. El-Rayes, (1987), "Microwave dielectric spectrum of vegetation - Part II: dual - dispersion model", *IEEE Transactions on Geoscience and Remote Sensing*, vol. GE-25, no. 5, pp. 550-557.

Wang, Yong, Marc L. Imhoff, David S. Simonett, (1989), "Radar modeling of mangal forest stands", to be pulished in *The Proceedings of the IGARSS'89*, Vancouver, Canada, July, 1989.

Table 3.1. Stand samples extracted from SIR-B images

Stands	Ground conditions	Samples (line * sample)	Total pixels
SGn	nonflooded	(10 * 10), (10 * 10), (11 * 6)	266
SGf	flooded	(4 * 12), (10 * 10), (12 * 12)	292
GSn	nonflooded	(7 * 20), (18 * 9)	302
GSf	flooded	(17 * 19), (5 * 12)	383
Gn	nonflooded	(10 * 10), (10 * 10), (10 * 5)	250
Gf	flooded	(7 * 25), (16 * 7)	287

SGn is a stand with Sundri dominant and with Gewa present for a nonflooded surface; GSn has Gewa dominant and with Sundri present on nonflooded surfaces; and so on (See also Table 3.2 for stand characteristics).

Table 3.2. DBH (cm) counts of each stand per hectare

Stands	Species	< 4.9	5.-9.9	10.-14.9	15.-19.9	20.-24.9	25.-29.9	30.-34.9	35.-39.9
SG	Sundri	42560	816	319	125	52	17	2	1
	Gewa	1340	493	250	72	16	5	0	0
GS	Sundri	42560	502	184	78	21	6	1	1
	Gewa	1340	1084	458	98	15	2	0	1
G	Sundri	42560	142	34	16	8	2	0	3
	Gewa	1340	1769	575	136	26	2	5	4

Source: Chaffey, et al., (1985).

Table 3.3. Regression models

Height (m) on diameter (cm) for Gewa

	Regression models	R^2 value
Gewa	Hg = 5.549 + 0.258 * Dg	0.505
Sundri	Hs = 4.769 + 0.414 * Ds	0.672

Canopy thickness (m) on diameters (cm)

	Regression models	R^2 value
Gewa	Cg = 1.840 + 0.188 * Dg	0.679
Sundri	Cs = 1.768 + 0.331 * Ds	0.589

Table 3.4. Mean canopy biomass (kg) per tree for each DBH segment

DBH segment cm	Species Gewa	Sundri
< 4.9	2.9	2.6
5.0 - 9.9	6.1	13.0
10.0 - 14.9	12.9	39.8
15.0 - 19.9	27.6	74.9
20.0 - 24.9	58.8	86.3
25.0 - 29.9	125.4	86.3*
30.0 - 34.9	267.5	86.3*
35.0 - 39.9	393.5	86.3*

*: Two sources of data were used to construct this table. In the field *canopy* biomass measurements were made by a NASA and Bangladesh Science Team in October, 1984. For that data, there were no Sundri trees whose DBHs were over 25.0 cm. The second source of data was Chaffey, et al., (1985), for the same area. They mapped the area into segments of different DBHs, including DBH's exceeding 24.9 cm. However, they did not derive any measurements of canopy biomass. On merging the two data sets, the three highest DBH segments, lacked canopy biomass data. The same values as for 20.0 - 24.9 cm were therefore employed.

Table 5.1. Conversion constants from DNs to dB for SIR-B images

	C_{1i}	C_{2i}
DT 120	3157.45	55.50
DT 104	4389.06	56.42

Formulas for conversion of SIR-B image DNs to σ^o in dBs is:

$$\sigma^o = 10^* \log[DN^2 - C_{1i}] - C_{2i}$$

where i = 1, 2, corresponding to I

Marc Imhoff (1988, personal comm

UNIVERSITY OF CALIFORNIA, SANTA BARBARA

BERKELEY • DAVIS • IRVINE • LOS ANGELES • RIVERSIDE • SAN DIEGO • SAN FRANCISCO

SANTA BARBARA • SANTA CRUZ

Geography Department
Research Division

SANTA BARBARA, CALIFORNIA 93106

May 11, 1989

Mr. M.C. Imhoff
Code 675, National Aeronautics and Space Admin.
Laboratory for Oceans
Space and Earth Sciences Directorate
Greenbelt, Maryland 20771

RE: NASA NAG 5-1010, "Improvement and Extension of a Radar Forest Backscatter Model"

Dear Mr. Imhoff:

Enclosed you will find three copies of the semi-annual report which is now overdue. Sorry for the inconvenience.

If you have any questions, or require additional

Figure 2.1. Gewa tree models (from Tomlinson, 1986)

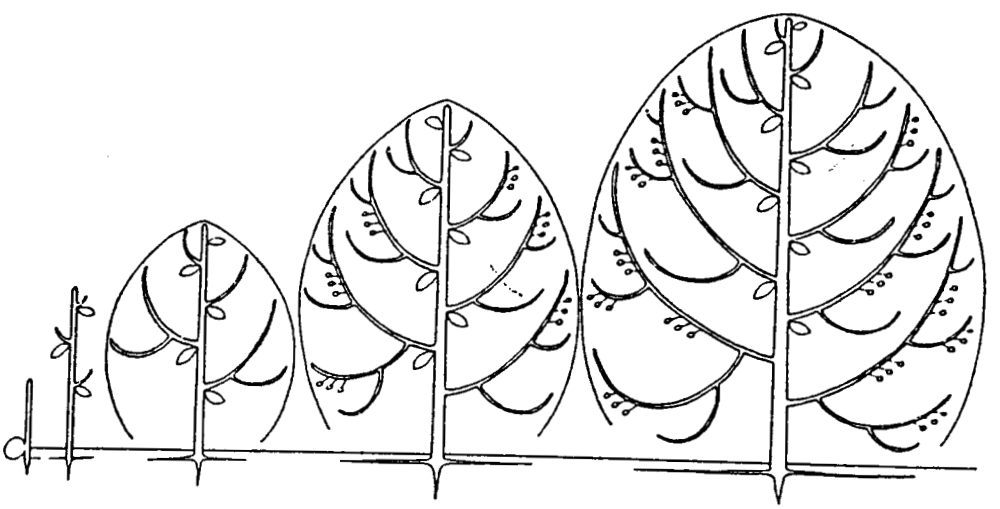

Figure 2.2. Sundri tree models (from Tomlinson, 1986)

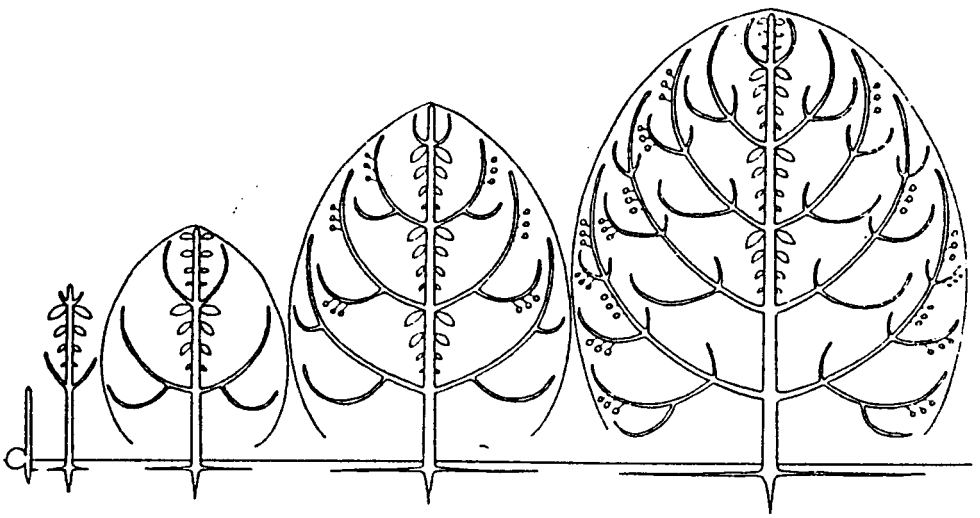

Figure 3.1. Model components of Sundri and Gewa forest stands

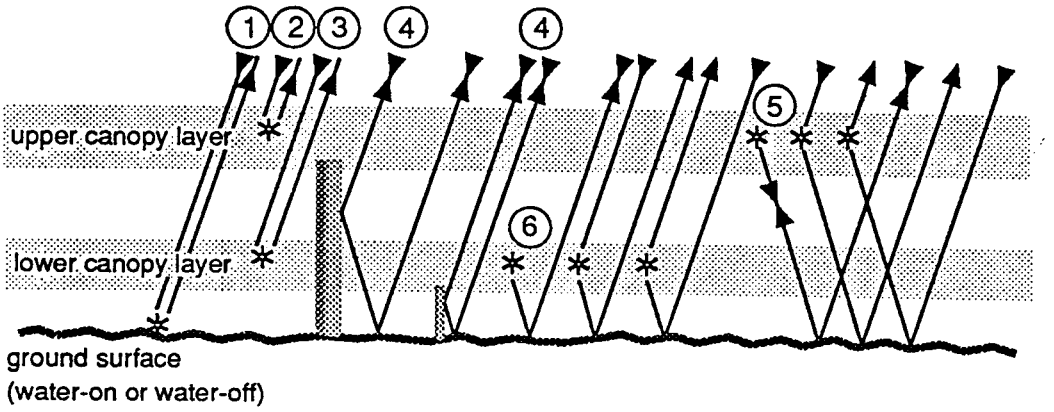

Figure 5.1. Boxplots of forest stands at 26° incidence angle

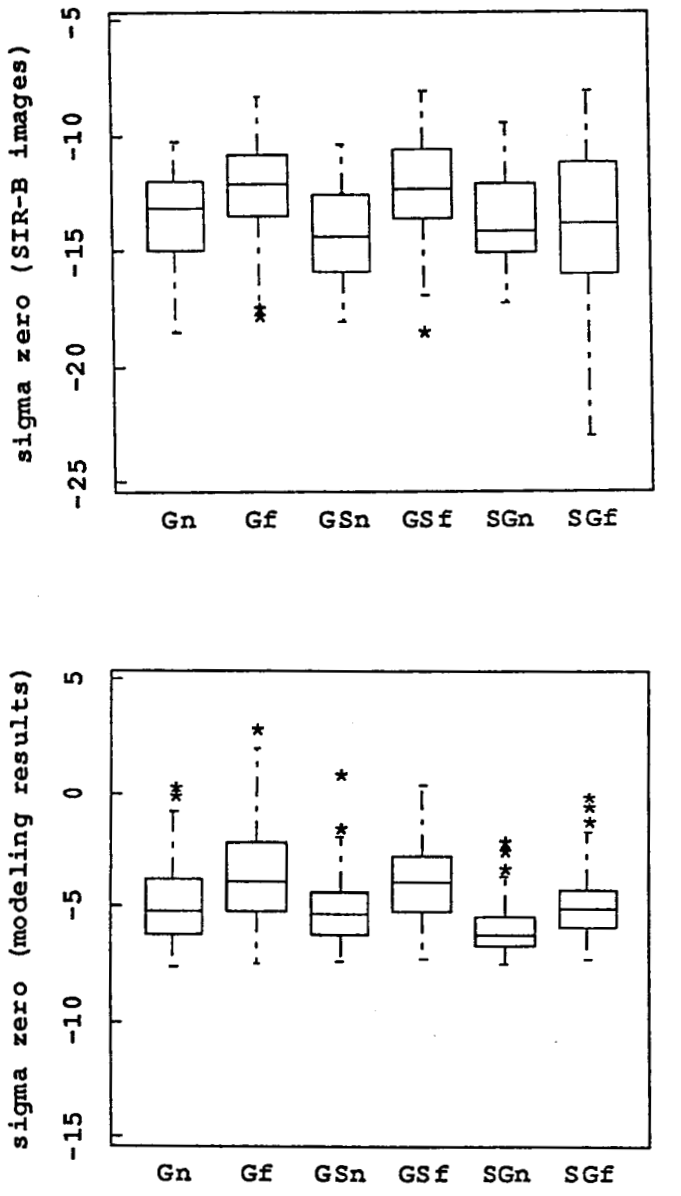

Figure 5.2. Boxplots of forest stands at 46° incidence angle